


Ionization-Induced Self-Channeling of an Ultrahigh-Power Subnanosecond Microwave Beam in a Neutral Gas

G. Shafir,¹ Ya. E. Krasik,¹ Y. P. Bliokh,¹ D. Levko,² Y. Cao,¹ J. G. Leopold,¹ R. Gad,¹ V. Bernshtam,³ and A. Fisher¹

¹*Physics Department, Technion, Haifa 32000, Israel*

²*Department of Aerospace Engineering and Engineering Mechanics, University of Texas, Austin, Texas 78712, USA*

³*Faculty of Physics, Weizmann Institute of Science, Rehovot 36100, Israel*

 (Received 28 October 2017; revised manuscript received 7 February 2018; published 28 March 2018)

Ionization-induced self-channeling of a ≤ 500 MW, 9.6 GHz, < 1 ns microwave beam injected into air at $\sim 4.5 \times 10^3$ Pa or He at $\sim 10^3$ Pa is experimentally demonstrated for the first time. The plasma, generated by the impact ionization of the gas driven by the microwave beam, has a radial density distribution reducing towards the beam axis, where the microwave field is highest, because the ionization rate is a decreasing function of the microwave amplitude. This forms a plasma channel which prevents the divergence of the microwave beam. The experimental data obtained using various diagnostic methods are in good agreement with the results of analytical calculations, as well as particle in cell Monte Carlo collisional modeling.

DOI: [10.1103/PhysRevLett.120.135003](https://doi.org/10.1103/PhysRevLett.120.135003)

The interaction of high-power, short-duration laser and microwave beams with plasma has been widely studied [1–5] due to intriguing physical phenomena involved and applications such as plasma particle accelerators [6,7], inertial confinement fusion [8], remote atmospheric sensing [9], high harmonic generation [10], etc. Laser guiding in plasma can be achieved either by self-channeling [11] or in a preformed plasma channel with a reduced plasma density near the axis [12].

The availability of subnanosecond high-power microwave sources of ≥ 1 GW at ≥ 10 GHz and electric fields ≥ 200 kV/cm has made it possible to study the nonlinear interaction of such electromagnetic (EM) waves with gas and plasma instead of lasers. This is important for understanding the phenomena underlying this process and for plasma heating, energy transfer, etc. Various phenomena were found to be responsible for EM pulse self-channeling [13,14], but, as a rule, the ionization process is of secondary importance, because the guiding profile of the refractive index appears as a result of the interaction of the preliminarily generated plasma with the EM beam. However, for certain conditions, the nonmonotonic dependence of the impact ionization cross section σ_i on the electron energy is sufficient for the EM beam's guiding [15,16]. The plasma density increases due to gas impact ionization as

$$\ln[n_e(r, t)/n_0] = n_g \int_0^t v(r, t') \sigma_i[w(r, t')] dt', \quad (1)$$

where n_0 is the natural background electron density ($\leq 10^5$ cm⁻³), n_g is the gas density, v and w are the electron velocity and energy, respectively, at the distance

r from the EM beam axis, and σ_i is the electron impact ionization cross section. The evolution of the plasma density for a Gaussian beam with the power distribution $P(r, t)$ with time normalized to the pulse duration t_{pulse} and r to the radial width r_{beam} is shown in Fig. 1. Typically, σ_i reaches its maximum at an electron energy of ~ 100 eV and decreases when the energy exceeds this value [17]. Thus, at the leading front of the EM beam, the density is maximal on axis. Later, when the wave amplitude becomes sufficiently large, the region with the highest ionization rate is shifted from the beam axis to its periphery, resulting in the formation of a plasma channel with minimal density at the beam axis.

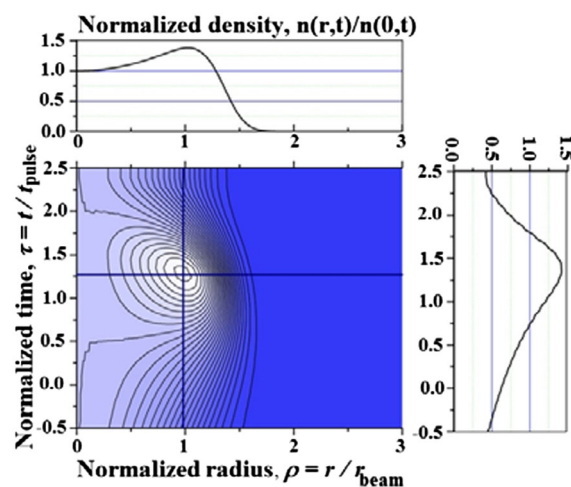


FIG. 1. Evolution of the plasma density $n(r, t)$, generated by an EM pulse. Plasma density is normalized by its value on the beam axis $\eta = n_e(r, t)/n_e(0, t)$, making the evolution of the density's radial profile more illustrative.

Such a plasma channel can be formed only when the wave amplitude exceeds a threshold value E_{thresh} , which can be calculated from Eq. (1) and the ionization cross section data. Helium and air are characterized by practically the same value $E_{\text{thresh}} \approx (4-5) \times 10^5 / \lambda$, where the electric field E_{thresh} and the wavelength λ are given in V/cm and in cm, respectively. For our microwave source $\lambda = 3$ cm, so $E_{\text{thresh}} \sim 150$ kV/cm. Equation (1) allows one to estimate the optimal gas pressure for the plasma channel formation to be $\sim 3 \times 10^3$ Pa.

In this Letter, we report the first observations of such self-guiding of a subnanosecond Gaussian, high-power (≤ 500 MW) microwave (9.6 GHz) beam in low-pressure $1.5-150 \times 10^2$ Pa gases (He and air).

The experimental setup is shown in Fig. 2. A super-radiance backward wave oscillator (9.6 GHz, ~ 500 MW, $t_{\text{pulse}} \approx 0.37$ ns) is connected to a horn antenna through a mode converter, producing a linearly polarized Gaussian beam [18]. The beam is focused using a hyperbolic dielectric (Ultem, $\epsilon_r \approx 3$) lens into a 100 cm long, 240 mm inner diameter Pyrex tube filled with He or air. The beam's characteristic radius at the antenna entrance plane is $r_{\text{beam}} \approx 7$ cm. At the focal plane, located at the distance of ~ 9 cm relative to the lens tip, the beam radius is $r_{\text{beam}} \approx 1.6$ cm, resulting in a Rayleigh length of ~ 5.4 cm and a maximal electric field of ~ 165 kV/cm for ~ 500 MW input power. Side and front views of the plasma light emission were obtained by a fast-framing (1.2 ns) 4QuikE intensified camera (Stanford Computer Optics).

To measure the intensity of the He spectral lines, an absolute calibrated setup consisting of mirrors, lenses, and a Chromex 250i imaging spectrometer (1800 grooves/mm, spectral resolution 0.3 Å/pixel) with a 4QuikE camera (Stanford Computer Optics) at its output was used. These measurements allow the determination of the energy level population of the excited atoms and ions and, respectively,

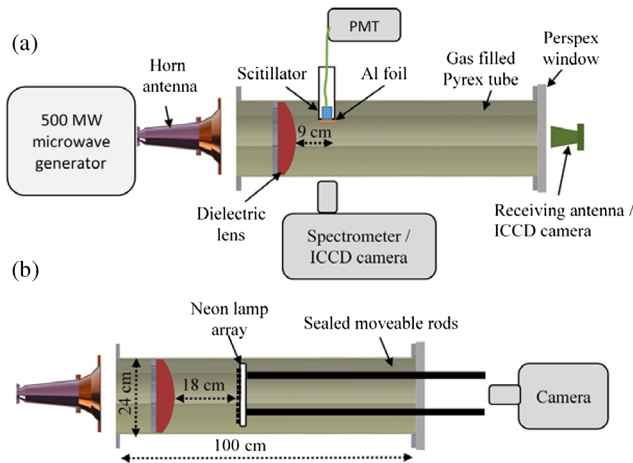


FIG. 2. Experimental setup. (a) The microwave, plasma light emission, and fast electron diagnostics; (b) microwave beam profile imaging using the Ne lamp array.

to calculate the density of atoms and ions using atomic data. The radial distribution of the transmitted microwave power at the Pyrex tube output was measured by a receiving antenna and recorded by a 12 GHz digitizing oscilloscope (Agilent DSO81024B). To measure the beam pattern, a Ne lamp (Multicomp, MC08020000) array consisting of 400 miniature tubes (4 mm in diameter) was placed inside the tube at the distance of 18 cm from the lens tip. The maximal energy of the plasma electrons was estimated by the electron-induced luminescence of an EJ-228 scintillator (0.5 ns rise and 1.5 ns decay times) with Al foils (10 and 20 μm thick) placed at its front surface together with the NIST tabulated continuous slowing down approximation range data (CSDA) [19]. The scintillator was coupled to an optical fiber connected to a Hamamatsu R7400U photo-multiplier tube placed inside a screen room.

Full 3D electromagnetic simulation in a vacuum (MAGIC [20]) shows that only $\sim 10\%$ of the incident power reaches the receiving antenna. Experimentally, it is found that for low ($P < 1 \times 10^3$ Pa) and high ($P > 1 \times 10^4$ Pa) pressures the transmitted power is close to this value, but there exists an intermediate pressure region, $1.5 \times 10^3 \text{ Pa} \leq P \leq 8 \times 10^4 \text{ Pa}$ for air and $7 \times 10^3 \text{ Pa} \leq P \leq 1.5 \times 10^4 \text{ Pa}$ for He, for which the microwave transmission seems to be blocked and the received power decreases by more than a factor of 2 (Fig. 3).

The microwave power waveforms normalized to the values in a vacuum, measured by the receiving antenna for 10^{-2} Pa (vacuum) and 4×10^3 Pa He, are shown in Fig. 3. In contrast to low or high pressures, at 4×10^3 Pa the transmitted microwave power has two peaks separated in time. Using our model of the plasma channel formation, this shape can be explained as follows. At the beginning of the pulse, when the wave amplitude is small, the plasma is generated mainly near the focal plane around the beam axis (Fig. 1). This profile of the plasma density enhances the radial divergence of the beam. The denser the plasma, the larger the beam divergence resulting in the decrease in

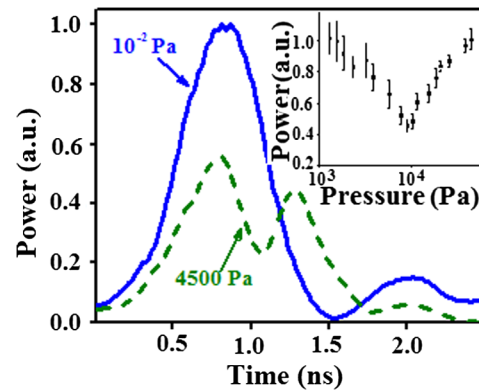


FIG. 3. The normalized microwave power measured by the receiving antenna for vacuum (10 mPa) and for He gas pressure of 4.5×10^3 Pa. Inset: Transmitted power vs He pressure.

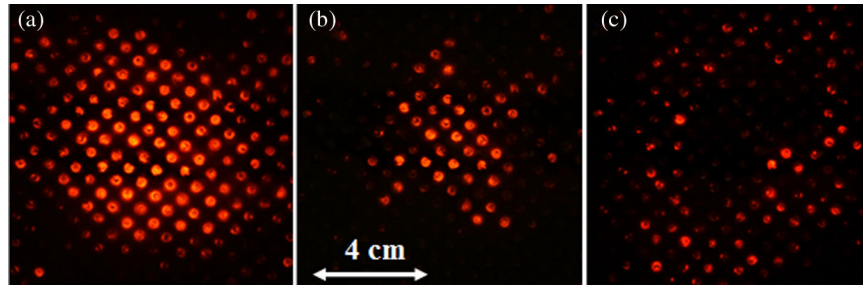


FIG. 4. The radial pattern of the microwave beam, obtained by time-integrated images of the Ne lamp array light emission at the distance of 10 cm from the focal plane for (a) vacuum; (b) 4.5×10^3 Pa, He; and (c) 3×10^4 Pa, He. The center of these images coincides with the beam axis.

the receiving antenna signal. Closer to the pulse maximum, when the wave amplitude is large, plasma is produced much faster at the beam periphery than on the axis. This density profile represents a channel with “walls” of denser (even overcritical) plasma, so that part of the diverged waves are captured in the channel and reach the antenna as a second maximum.

This microwave beam self-channeling was also confirmed by the beam transverse pattern recorded by the array of Ne lamps (Fig. 4). For a vacuum, the pattern diameter was ~ 9 cm, which agrees with the expansion of the Gaussian beam after its focal plane obtained both analytically and by MAGIC simulations (see Ref. [18]). When the tube was filled with He at 4.5×10^3 Pa, the pattern diameter decreased to ~ 4 cm [Fig. 4(b)], which indicates that only the central part of the beam propagated to this point. Increasing the pressure to 3×10^4 Pa results in a hollow pattern [Fig. 4(c)], indicating that an overdense plasma close to the axis blocks microwave transmission except at the beam periphery. Similar patterns are obtained for air but at different pressure values.

The side view of the time-integrated plasma light emission obtained by a digital camera is shown in Fig. 5. One can see that, between the lens and focal plane, the plasma profile follows the focusing beam. However, beyond the focal plane, the light emission shape differs from the expanding beam and forms an ~ 40 cm long (~ 7 times the Rayleigh length) conelike channel. The beam creates an electric field of ~ 165 kV/cm sufficient for channeling, only near the focal plane, where a hollow structure of the density distribution is formed. Further

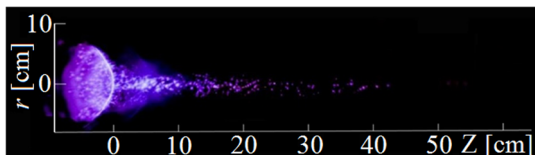


FIG. 5. Side view of the time-integrated light emission from the plasma (He at 4.5×10^3 Pa). $z = 0$ is at the dielectric lens tip, and the large circular region for $z < 0$ is the flashover along the lens surface.

downstream, the beam diverges, the field decreases below the critical value, and the plasma is created mainly near the axis. Nevertheless, even a short “plasma channel” near the focal plane decreases the beam divergence and enhances the plasma density near the axis by self-focusing.

To verify that the plasma buildup is not altered by the lens flashover, the plasma light emission evolution was also studied using the 4QuikE camera (Fig. 6). Here $t = 0$ corresponds to the time when the light emission begins, which is delayed by ~ 1 ns relative to the time the beam enters the tube. The plasma is first generated at the focal location. Then, within ~ 1 ns, it spreads in the forward direction and back towards the lens. The latter was explained in Ref. [21] by the reflection of the EM waves from the focal region, where the density approaches the critical value. Since $t_{\text{pulse}} < 1$ ns, the plasma formation at the lens surface does not affect the beam’s forward propagation.

Front view images of the plasma channel when the camera focus was aligned to the focal plane show a hollow central region in the light emission pattern for He at 4.5×10^3 Pa [Fig. 7(a)] and air at 10^3 Pa. A sequence of plasma light emission images with a 1 ns time delay

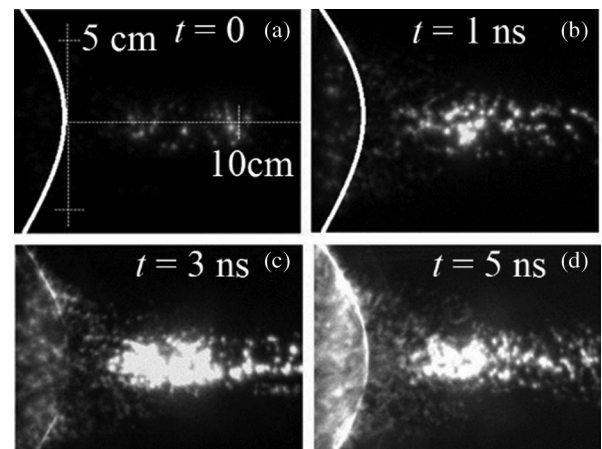


FIG. 6. Side view framing (duration of 1.2 ns) images of the plasma, obtained at different times in 4.5×10^3 Pa, He. The focal plane is at the distance of ~ 9 cm from the lens tip. The lens boundary in the upper frames is drawn for clarity.

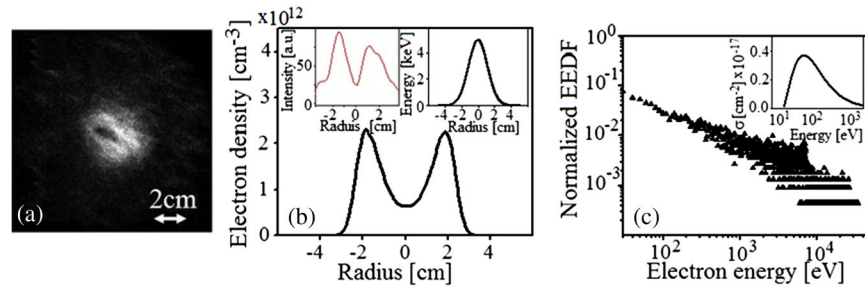


FIG. 7. (a) Front view framing image (frame duration of 1.2 ns) of the light emission from the plasma (4.5×10^3 Pa, He) at $t = 0$ ns. (b) 1D PIC calculated radial distribution of the plasma density at the focal plane at the peak of the microwave field. Right inset: The calculated radial distribution of the electron energy. Left inset: Line profile of the intensity distribution shown in (a). (c) The 1D PIC calculated EEDF at the peak of the microwave field. Inset: The electron impact ionization cross section vs the electron energy [17].

between frames shows that the hollow structure fills in within ≤ 1 ns. These data agree with the emission patterns obtained by the array of Ne lamps (Fig. 4) and present an additional indication that at these pressures the beam propagates only close to the axis. For the microwave power of ~ 500 MW, the simulated by MAGIC electric fields in a vacuum at the focal location are ~ 165 kV/cm on the beam axis and ~ 25 kV/cm at $r = 3$ cm. Thus, the electron energy decreases ~ 36 times from the axis to the beam periphery, so that the plasma density builds up faster and becomes denser at the periphery than along the beam axis. This radial density distribution suggests that a guiding plasma channel forms in which the beam propagates with reflections from the larger density plasma boundary just like in an “optical fiber.”

A numerical study of the plasma formation at the focal plane was carried out using 1D particle in cell (PIC) Monte Carlo collisional simulations [22]. The plasma was generated by the electron impact ionization of He or air started by 10^5 cm⁻³ density seed electrons. The modeling accounted for the electron-neutral momentum transfer collisions, excitation of electronic levels of neutrals, and ionization. The simulations show that, in He at 4.5×10^3 Pa, the plasma density reaches $n_e \approx 2.3 \times 10^{12}$ cm⁻³ at $r = 2$ cm and $n_e \approx 6 \times 10^{11}$ cm⁻³ at $r = 0$ after 0.8 ns from the pulse turn on [Fig. 7(b)]. The electron energy distribution function (EEDF) at that time shows that the electrons reach energies of the order of tens of keV [Fig. 7(c)]. The radial distribution of the plasma density agrees qualitatively with experimental data [left inset in Fig. 7(b)]. The critical density necessary for the microwave cutoff is $n_{cr} = 1.2 \times 10^{12}$ cm⁻³, so that only the central part of the beam can propagate through the plasma, and is reflected from the overdense plasma, formed at the beam periphery. A similar result was obtained for air at 10^3 Pa. In addition, the simulations show that for lower or higher gas pressures, when the pulse duration exceeds 1 ns, or when the amplitude of the electric field is < 150 kV/cm, no channeling develops and the resulting plasma density’s radial distribution remains Gaussian-like. These parameters agree with those predicted by Eq. (1).

The electron energy was estimated using the luminescence generated by the electrons in plastic scintillators covered by light-blocking thin Al foil [Fig. 8(a)]. The luminescence emission with up to $20 \mu\text{m}$ thick aluminum foil can be excited only by electrons with an energy ≥ 15 keV [19].

In the 1D PIC simulations, the plasma buildup continues after the microwave beam termination, and within 2 ns, the density increases up to $n_e \approx 10^{14}$ cm⁻³. To verify these high ionization rates, the plasma density was estimated using the absolute calibrated spectroscopy system, which allows the measurement of the density $\geq 2 \times 10^{13}$ cm⁻³. The measured spectral lines FWHM were almost equal to the instrumental broadening, and hence Doppler and Stark broadening are negligibly small [Fig. 8(b)]. The population of excited He I $1s3d(^3D)$, $1s3d(^1D)$, $1s3p(^3P)$ $1s4s(^1D)$, and $1s4d(^1D)$ levels was derived from the line intensities and compared with the results of time-dependent collisional radiative modeling [23] of the corresponding level population. This modeling was carried out with the time-dependent EEDFs obtained from the 1D PIC simulation. The plasma density found by this method was $\geq 10^{14}$ cm⁻³, which agrees well with the value of the density obtained by 1D PIC simulations at $t > 2$ ns.

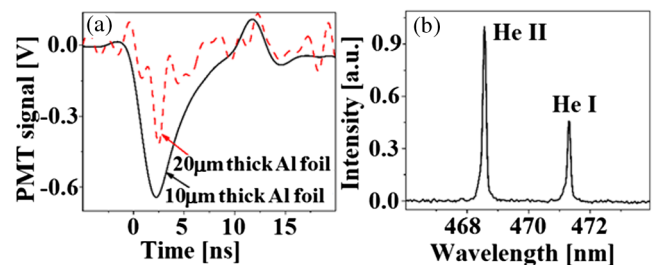


FIG. 8. (a) The luminescence signal from the fast plastic scintillator covered by Al foil, at $r = 4.5$ cm from the axis at the focal plane. (b) Typical measured spectral lines of He I (471.3 nm) and He II (468.7 nm) at 4.5×10^3 Pa. The frame duration of the 4QuikE camera was 10 ns.

In conclusion, the experimental results show ionization-induced self-channeling of a short pulse, high-power, focused microwave beam, injected into a gas for the first time. The guiding of the beam along a few Rayleigh lengths occurs due to the larger oscillating electron energy and, respectively, slower ionization rate at the beam axis than at its periphery. The data obtained using optical and spectroscopic methods agree with the 1D PIC simulations and analytical modeling.

The authors are grateful to Professor Edl Schamiloglu for fruitful discussions and S. Gleizer, J. Gleizer, and E. Flyat for kind technical assistance. This work was supported in part by the PAZY Grant No. #2020960.

-
- [1] Y. Ehrlich, C. Cohen, A. Zigler, J. Krall, P. Sprangle, and E. Esarey, *Phys. Rev. Lett.* **77**, 4186 (1996).
- [2] S.-Y. Chen, G. S. Sarkisov, A. Maksimchuk, R. Wagner, and D. Umstadter, *Phys. Rev. Lett.* **80**, 2610 (1998).
- [3] P. Sprangle, E. Esarey, J. Krall, and G. Joyce, *Phys. Rev. Lett.* **69**, 2200 (1992).
- [4] M. S. Hur, J. S. Wurtele, and G. Penn, *Phys. Lett. A* **372**, 3452 (2008).
- [5] M. Châteauneuf, S. Payeur, J. Dubois, and J. C. Kieffer, *Appl. Phys. Lett.* **92**, 091104 (2008).
- [6] E. Esarey, C. Schroeder, and W. Leemans, *Rev. Mod. Phys.* **81**, 1229 (2009).
- [7] W. P. Leemans *et al.*, *Phys. Rev. Lett.* **113**, 245002 (2014).
- [8] M. Tabak, J. Hammer, M. E. Glinsky, W. L. Kruer, S. C. Wilks, J. Woodworth, E. M. Campbell, M. D. Perry, and R. J. Mason, *Phys. Plasmas* **1**, 1626 (1994).
- [9] H. L. Xu and S. L. Chin, *Sensors* **11**, 32 (2011).
- [10] Y. Tamaki, J. Itatani, Y. Nagata, M. Obara, and K. Midorikawa, *Phys. Rev. Lett.* **82**, 1422 (1999).
- [11] G.-Z. Sun, E. Ott, Y. C. Lee, and P. Guzdar, *Phys. Fluids* **30**, 526 (1987).
- [12] D. J. Spence, A. Butler, and S. M. Hooker, *J. Opt. Soc. Am. B* **20**, 138 (2003).
- [13] P. Sprangle, C. M. Tang, and E. Esarey, *IEEE Trans. Plasma Sci.* **15**, 145 (1987).
- [14] F. W. Perkins and E. J. Valeo, *Phys. Rev. Lett.* **32**, 1234 (1974).
- [15] Y. L. Bogomolov, S. F. Lirin, V. E. Semenov, and A. M. Sergeev, *JETP Lett.* **45**, 680 (1987).
- [16] A. G. Litvak, in *Proceedings of the International Workshop on Strong Microwave Plasmas* (Institute of Applied Physics, Russian Academy of Sciences, Nishny Novgorod, 1991), pp. 267–286.
- [17] Y. Ralchenko, R. K. Janev, T. Kato, D. V. Fursa, I. Bray, and F. J. de Heer, *At. Data Nucl. Data Tables* **94**, 603 (2008).
- [18] G. Shafir, A. Shlapakovski, M. Siman-Tov, Y. Bliokh, J. G. Leopold, S. Gleizer, R. Gad, V. V. Rostov, and Y. E. Krasik, *J. Appl. Phys.* **121**, 033301 (2017).
- [19] M. J. Berger, J. S. Coursey, M. A. Zucker, and J. Chang, NIST, <http://www.nist.gov/pml/data/star/index.cfm>.
- [20] B. Goplen, L. Ludeking, D. Smith, and G. Warren, *Comput. Phys. Commun.* **87**, 54 (1995).
- [21] Y. Y. Brodskii, S. V. Golubev, V. G. Zorin, A. G. Luchinin, and V. E. Semenov, *Sov. Phys. JETP* **57**, 989 (1983).
- [22] D. Levko, S. Yatom, V. Vekselman, J. Z. Gleizer, V. T. Gurovich, and Y. E. Krasik, *J. Appl. Phys.* **111**, 013303 (2012).
- [23] Y. V. Ralchenko and Y. Maron, *J. Quant. Spectrosc. Radiat. Transfer* **71**, 609 (2001).